Analog Integr Circ Sig Process
DOI 10.1007/s10470-006-8737-x

CMOS image sensors for sensor networks

Eugenio Culurciello · Andreas G. Andreou

Received: 27 October 2005 / Revised: 6 April 2006 / Accepted: 10 April 2006 / Published online: 27 June 2006

Abstract We report on two generations of CMOS image sensors with digital output fabricated in a 0.6 μm CMOS process. The imagers embed an ALOHA MAC interface for unfettered self-timed pixel read-out targeted to energy-aware sensor network applications. Collision on the output is monitored using contention detector circuits. The image sensors present very high dynamic range and ultra-low power operation. This characteristics allow the sensor to operate in different lighting conditions and for years on the sensor network node power budget.

Keywords Image sensor · CMOS · Sensor network · ALOHA · Low-power imager · Address-event

1. Introduction

Recent trends towards parallel and distributed processing in wireless sensor networks necessitate the re-thinking of interfaces for sensor and sensory applications, or in other words, of *sensor and network co-design*. The task in such networks is not necessarily the precise restitution of video or audio information but rather information extraction from an array of sensors. In a sensor network requiring an electronic image sensor as interface, commercial off-the-shelf (COTS) image sensors are not able to efficiently extract features in a scene, because they *blindly* collect all the visual information whether the scenes contains new and useful data or not. In other words they operate as a camera taking snapshots. If data reduction is not performed at the sensor level, software techniques must be used [1–3]. In this case, the amount of computation to extract features from the visual data is practically always too high for the limited power budget of a sensor network node.

Conventional scanned image sensors [4–6] do not make efficient use of the available output bandwidth, since much of the pixels' data can be read before having integrated sufficient light. For example a dark pixel returning a digital value of 0 after light integration will use 8 bits during output communication to transmit no information whatsoever! Collecting useless information not only wastes energy at the sensor level, but also at the node and network level, since the uninteresting information is broadcasted to the network. Sensors need to be more efficient in reducing the data during the gathering phase, before communicating it to the sensors network node for further processing. Instead of taking snapshots, image sensor network have to collect feature sets useful to a specific task.

In a distributed processing system, when there is a-priori knowledge that not all nodes are likely to require computation and communication resources at the same time, a fixed time-slot (synchronous) allocation of resources among all nodes is wasteful. If the demand for resources is bursty, computation and communication can be done asynchronously. This is the reason that a wealth of research is underway to develop new protocols for communication in wireless sensor networks that are energy-aware [7]. A excellent example of sensor and network co-design is given by P. Julian [8].

Address-event image sensors report high communication efficiencies at the cost of additional circuit components and a

E. Culurciello (✉)
Department of Electrical Engineering, Yale University,
New Haven, CT 06520, USA
e-mail: eugenio.culurciello@yale.edu

A. G. Andreou
Department of Electrical Computer Engineering,
Johns Hopkins University, Baltimore, MD 21218, USA
e-mail: andreou@jhu.edu

slight increase of the power budget [9–11]. We thus propose to use the simplest access protocol, the ALOHA protocol [12], in conjunction with efficient ways to detect output bus contention. The marriage of these two techniques results in one of the lowest power, wide dynamic-range address-event image sensor reported in the literature. The imager has a lower power budget than previously reported image sensor aimed at smart-dust networks [13] and remote smart sensors [14].

1.1. Why the need of more image sensors?

Many CMOS image sensors are available on the market but their power budget is often too high for the limited power available at the sensor network node [15–17]. These power levels are comparable to the power consumption of a transmitting sensor network node and are thus unsuitable for prolonged field operation. In addition, commercial image sensors provide a series of features (color processing, compression, multiple standard outputs) that are of little significance to sensor network nodes, where low power consumption is instead a much more desirable feature. COTS image sensors provide high resolutions (VGA or megapixel), while in sensor networks, and especially in wake-up detectors, multiple QCIF or quarter-VGA sensors are sufficient [18, 19].

COTS modules can last only 1 day running on two AA batteries, while measured data from custom image sensors in research papers yields 6 days [20], 13 days [6], and 4.5 years for our most recent prototype presented here. Our sensor use an insignificant amount of power when compared to the transmitting node power and thus allow for continuous operation as wake-up detectors.

The lack of proper image sensors has slowed down the deployment of vision-based sensor networks. The image sensors here reported eliminate redundant data at the image sensor (hardware) level, instead than at the processor execution level. By avoiding the communication of unnecessary data, more bandwidth will also be available at the network level. The operation of the image sensor can be prolonged to years, as opposed to only hours when using COTS sensors. Consequently the deployment and maintenance of vision-based sensor networks can be easier and cheaper. In addition, the image sensors here reported are inexpensive in mass-production, because of the reduced pixel count and small die sizes.

1.2. Recent work on image sensor network

Few groups are trying to instrument sensor networks with image sensors. Most of these groups are working with COTS image sensors and additional processing hardware to develop a image sensor board for COTS sensor networks nodes. One of such groups is UCLA and Agilent with the design of the Cyclops sensor networked camera [21]. The Cyclops design employs an external processor, CPLD, SRAM and FLASH memory, offering CIF-resolution image processing at the expense of large power consumption (excess of 50 mW). Another group using COTS camera is led by Nina Berry at Sandia National Laboratories [22]. This group uses a PASTA USC ISI board, which consumes 300 mA at 9 V (2.7 W) [23]. Needless to say, these systems cannot be mobile and autonomous for the extended periods of time typical of sensor network applications as environmental monitoring [24–28], safety and defense [29, 30], robotics [31] and traffic control [32].

1.3. Paper organization

In this paper we present two generation of digital image sensors prototypes targeted for sensor networks applications: *ALOHAim1* and *ALOHAim2*. ALOHAim1 is a 32×32 pixel array [33], ALOHAim2 is a 64×64 pixel array organized as four independent quadrants of 32×32 pixels. In Section 2 we introduce the system architecture of the image sensors, in Section 3 we present the results collected by the image sensors and their performance. Finally in Section 4 we discuss the results and the applications in sensor networks. A summary is given in Section 5.

2. System architecture

2.1. Address-event representation

The image sensors here presented utilize an event based digital representation (AER) of information originally proposed by Mahowald and Sivilotti [34, 35] and subsequently re-engineered by Boahen [9]. Several address-event image sensors have been reported in the literature [10, 11, 36–38].

In the AER terminology, *events* are communication primitives sent from a sender to one or more receivers. For an image sensor, events are individual pixels reaching a threshold voltage and accessing the bus for communication with an outside receiver. An AER image sensor is composed of an array of pixels, and the digital output of the image sensor is the address of the pixel that is to communicate an event.

The integration time of each pixel varies in relation to the incident light intensity. Since the activity of the array is generated by the light intensity of the scene, and not an external scanning circuitry, the rate of collection of frames can be modulated by varying the *request-acknowledge* cycle time between the imager and the receiver circuitry. *Thus information can be extracted on demand from individual nodes in a wireless sensor network*. The address-event representation of an image can be thought as a realization of a delta-sigma pixel-parallel analog to digital converter [20].

Fig. 1 ALOHA image sensor in a sensor network node

In this paradigm the output of the ALOHA image sensor is a sequence of delta-sigma conversion, identified by the addresses of individual pixels. Thus the output of each pixel of the image sensor is always 1 bit and is only communicated when enough light (information) has been collected. This corresponds to a dynamic allocation of the output bandwidth determined by *need* as opposed to sequential scanning, which allocates communication bandwidth uniformly but inefficiently across pixels. Thus, representing intensity in the time domain allows each pixel to have large dynamic range [5, 10, 39, 40].

Referring to Fig. 2, the pixels readout initiates with a *request* (Req) from the image sensor array to the receiver circuitry. This request occurs after a pixel has generated an event. The requesting pixel will activate the row and column ROM that output its address on the bus. The request signal enables the output or a OR gate for both the row and column of the generating pixel. The receiver responds with an *acknowledge* signal (Ack) after reading the pixel address. This output modality corresponds to a *row-column* organization.

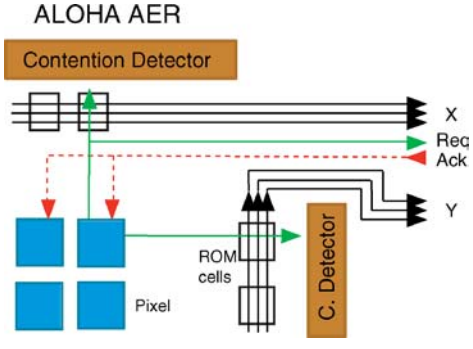

Fig. 2 ALOHA image sensors architecture. A pixel generates an event after collecting light, and rises a request signal (*Req*). The request activates a ROM cell in both row and column. The ROM encodes the pixel *X*, *Y* address and outputs in on the bus. A collision detector circuit detects multiple rows or columns trying to access the output bus at the same time. The collision detector circuits is reported in Fig. 6. The receiver circuits responds with an acknowledge (*Ack*) as a confirmation of detecting the event and reading the image sensor output data (the originating pixel address)

In other words the active pixel initiates communication on the output bus with independent requests on both *X* and *Y* address buses. Pixel act independently from each other and can generate requests and access the bus at any time. Row-column organization of the image sensor improves read-out speed by eliminating the large capacitance associated with the array common output bus lines. This capacitance is encountered when a request is performed within the whole array. Figure 2 shows the architecture of the row and column arbitration circuits in the unfettered ALOHA image sensors. Notice that since there are many pixels in one image sensor and only one output channel, an access circuit is required. The ALOHA access technique is used in our sensors to resolve contention on the bus access. ALOHA access allows individual transmitters, in this case pixels, to write data on the bus as soon as data is available. In other words pixel are allowed to initiate communication without any arbitration or queueing between them and the bus. This access reduces the latency of communication at the expenses of collisions, since multiple pixel might access the bus at the same time and produce garbage data on the bus. The ALOHA access technique was initially used for computer network and the early stages of the internet at University of Hawaii (hence the name). This access technique was chosen for its high performance compared to popular techniques [33, 41], especially for the small image sensor arrays used in sensor network applications.

Image data from our sensors can be reconstructed in two possible ways [10]:

- *Histogram reconstruction*: Counting events and reconstructing an histogram of the events in the array. This corresponds to an array proportional to light intensities onto each pixel.
- *Inter-event reconstruction*: Waiting for two consecutive events for each pixel in the array and then computing the inter-event time between such two events.

An optional external timer can index each event and compute the inter-event difference, which is inversely proportional to the light intensity. An external buffer must hold the latest pixel time index and the intensity value.

Sensor ALOHAim1 is a 32×32 pixel array which provides 10 bit output (5 bit for each row and column address), a request and acknowledge signal, plus an additional and optional two bits for row and column digital collision detection [33]. The image sensor uses three power supplies: analog (V_{dda}) and digital (V_{ddd}) supply plus a pixel reset supply (V_{ddr}). The supplies can be used independently or tied together. The sensor was designed for 3.3 V operation.

The sensor ALOHAim2 provides an identical interface as ALOHAim1, but the fabricated chip is organized as four quadrants of 32×32 pixels. Each quadrant can be read independently using four independent ALOHA channels. This

organization allows to change the quadrant of attention without increasing the pixel rate or using more readout bandwidth.

2.2. Digital pixel

The digital pixel employed in the design of the ALOHA image sensors improves on the *integrate-and-fire pixel* [42] and on subsequent design of event-generating pixels [10, 11]. The integrate-and-fire pixel operates by integrating the small photo currents on a capacitor, until the voltage exceeds a threshold. At that time, the pixel transmits an event at the periphery of the array. A disadvantage of this pixel is its high power consumption due to the input slew rate. A current-feedback event-generator improves the power consumption by 4 orders of magnitude [10]. The pixel used in the ALOHA image sensors improves on the low power design of the current-feedback event generator by removing two inverters in pixel. This improvement results in a even lower power consumption during event generation and in the silicon area used by individual pixels. A typical digital inverter using minimum size transistors, in a 0.5-m process and 3.3-V supply, consumes only about 0.06 pJ (40 μW $\times$ 3 ns $\times$ 0.5) per off-transition (rising input, falling output) and about 0.18 pJ (120 μW $\times$ 3 ns $\times$ 0.5) per on-transition (falling input, rising output). Therefore eliminating two inverters in the design allowed us to save 0.24 pJ/event produced by the pixel. In a total power consumption of 3.88 pJ/event [10, 11], the savings amounts to 6% of the total power budget per event.

Active pixel or analog pixel sensor (APS) [6, 43] have traditionally employed analog buffering and transmission of information from the pixel array to the periphery. In contrast digital pixel sensors (DPS) [10, 44] quantize the analog pixel value and provide digital data conversion at the pixel level. Figure 3 shows the schematic of the pixel. It includes asynchronous circuitry that generates an event or request and resets the voltage on the capacitor when the request is acknowledged (AE digital circuitry). The operation of the pixel is divided into three main phases. First the light is converted into a current by the photodiode; this current discharges the integrating capacitor. The integrated voltage is then converted into a 1-b pixel request ($\sim$*Req*) signal and finally, after the communication cycle on the output bus, the pixel is acknowledged (*Ack*) and reset.

The photons collected by the *n*-type photodiode are integrated on a 120 fF capacitor, resulting in a slew-rate of 0.083 V/ms in typical indoor light conditions (0.1 mW/cm^2). Because the slew-rate can be very small in presence of low lighting conditions, the comparator for generating the pixel request signal must have a fast switching time with low power consumption. The pixel uses an inverter with positive current feedback, shown in Fig. 3, to produce a digital pulse that activates the signal $\sim$*Req*. To reduce power, the integration capacitor is disconnected from the comparator when a request is generated [10].

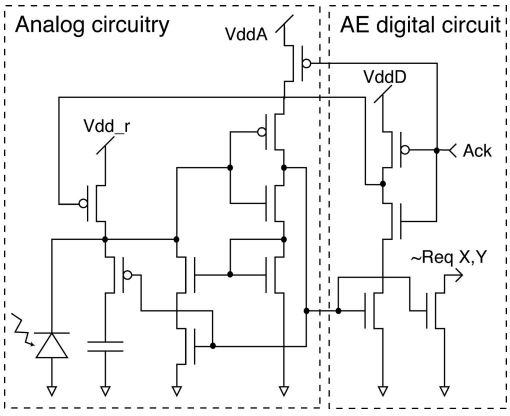

Fig. 3 Pixel schematic of the ALOHA image sensors. The analog portion is a current-feedback event generator circuit, the digital circuit is an asynchronous interface to the output bus

The digital circuit that generates the pixel request and receives the acknowledge/reset signal is shown in the right part of Fig. 3. When the comparator is triggered, a row and column request ($\sim$*Req*) is generated to access the unfettered output bus.

The pixel can operate with as low as 2.1 V and up to 5 V. The limiting factor in operating this pixel at a lower voltage is the current-feedback event generator circuit. This circuits employs an output stage with reduced swing due to the current mirror.

2.3. An analog contention detector for ALOHAim1

An ALOHA array of sensory cells with unfettered access to a common output bus from can cause collision, lowering the bus throughput [12]. The proposed image sensor employs a simple and effective way to detect contentions when multiple pixels access the channel at the same time. This implementation is a great simplification of older and more convoluted approaches [45, 46]. In this way, conflicting transmission can be detected and the data discarded. For sensor network monitoring applications and for low collision rates, this loss of data is negligible. The ALOHA image sensors use two contention detector circuit: one for the rows and one for the column collisions. The two collision detectors are pictured in Fig. 2 (CD). This allows to detect separate row and column collision.

In ALOHAIm1 we use an analog circuit to detect multiple requests on the output bus control line, using the circuit in Fig. 4, which is a modified multi-threshold digital NOR gate [33]. The principle of operation is to size and bias the NOR circuit so that it operates with multiple thresholds. In a digital NOR every single one input being high will make the output commute to low. By creating two logic threshold in the NOR

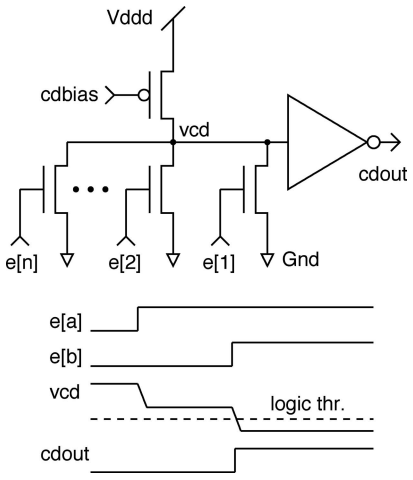

Fig. 4 Analog contention detector circuit for ALOHAim1. Signals *e* are row or column pixel requests. The detector operates using a multi-value logic NOR gate: when one *e* is high, *cdout* is high, when two or more *e* are high *cdout* is low and collision is detected

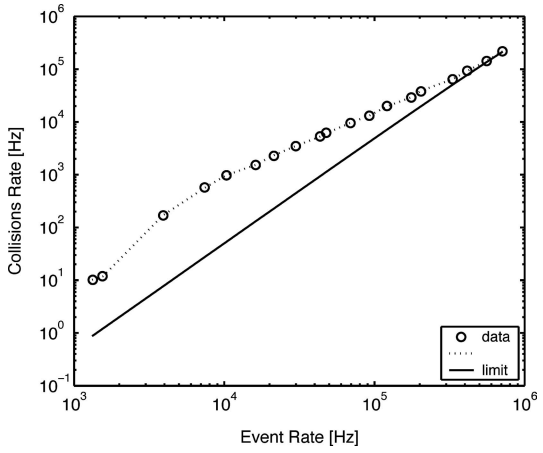

Fig. 5 Measured contention rate versus load and its ALOHA theoretical limit for image sensor ALOHAim1

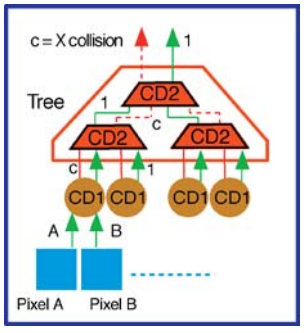

Fig. 6 Digital contention detector circuit for ALOHAim2. Since the pixel sends the request signal to both row and columns, here we only report the column circuit. The row circuit is identical, but operated in the vertical right side of the array, as portrayed in Fig. 2. CD1 and CD2 are the circuits in Fig. 7. The signal *X collision* is the column collision detector output

circuit, we can detect one or more input high. This is done sizing the transistors in the circuit so that if only one input is high, the output of the NOR will still be above the threshold of the following digital gates. If more that one input is high at a certain time, the output of the NOR will fall below the logic threshold and thus constitute a contention detection signal.

Referring to Fig. 4, signals *e* are the row or column pixel requests. When a single pixel requests the bus with signal $e[a]$ the internal voltage of the contention detector *cd* remains below the threshold of the following logic stages. As a second pixel request the bus before transmission of the previous one has been completed, signal $e[b]$ will bring *vcd* below the logic threshold and thus enable the output of the contention detector *cdout*.

The collision rate as a function of the event rate (also called *offered load*) is shown in Fig. 5, together with the theoretical limit f_{coll} reported in Eq. (1).

$$f_{coll} = f_{ev}(1 - e^{-2\alpha f_{ev}/f_{\max}}); \quad (1)$$

In Eq. (1) f_{ev} is the pixel's event rate, α is the portion of pixel active and $f_{\max}$ is the imager maximum event rate. Data was collected by varying the uniform light intensity falling onto the image sensor. This corresponds to varying the event rate to the sensor. As a results of increasing the load, the collision rate increase as expected by the theory [12, 41, 47]. The collision rate data is higher than the theoretical limit at low rates because of the temporal correlation between events due to the bursty read-out. For this reason pixel start to integrate almost at the same time and therefore have an higher chance to collide.

The power consumption of this contention detector circuit is dominated by the static power consumption of the pseudo-CMOS logic. Here a large bias current was used (20 μA) for high speed operation. This account to 66 μW operating at 3.3 V and 10 Kevents/s.

2.4. A digital contention detector for ALOHAim2

A major power reduction improvement in the performance of ALOHAim2 was achieved by using a digital realization of the collision detector. The analog collision detector of Section 2.3 requires a bias current to operate, and this current is proportional to the operating speed.

The digital collision detector of ALOHAim2 is presented in Fig. 6. The circuit is organized as two separate one dimensional circuits in a row-column arrangement. The collision detector works in a binary tree arrangement, where the leaves are individual pixel and the output of the tree is the collision detection signal. Referring to Fig. 7, the top circuit is the first layer of the collision detector (CD1) which serves as interface for two pixel in the array (leaves 'A' and 'B' in Fig. 6). This first layer outputs a logic one only on the output labeled '1' if there is no collision and only a single event is present between leaves 'A' and 'B'. Otherwise output 'c' will identify a collision on two neighboring pixels. The bottom circuit (CD2) is one branch of the digital tree which takes input ('c1', 'c2', '11', '12') from two first-layer circuits (Fig. 7, top). The output of the second layer is the same as the first

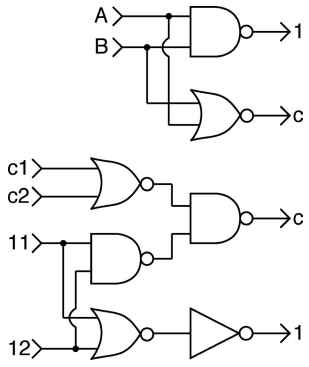

Fig. 7 Digital contention detector circuit for ALOHAim2: a two pixel interface CD1 (top) and two-couples interface CD2 (bottom)

layer circuit: if one collision occurs 'c' will present a logic one. Output '1' will present a logic one only if a single event occurred at the previous two leaves. The following layers of the tree use the circuit CD2. The tree layers are $log_2(N)$ (where 'N' is the number of pixel in one dimension of the array) and the final layer presents on output 'c' the collision detection output.

Notice that this digital realization of the collision detector uses no static power, since it is designed with static digital gates. Also it is fast, since it involves $1 + 2log_2(N)$ fully static digital gates to resolve a collision. This implementation is three orders of magnitude more power-efficient than the analog collision detector of Section 2.3 and other approaches [45, 46].

The output of the digital collision detector is given in Fig. 8, where the collision (C) on the array are monitored as a function of the event rate f_{ev} from one quadrant of the ALOHAim2 image sensor. Here only the collision for low event rate have been measured, since these are typical event rates if the sensor is used in a sensor network operating indoor. C, the solid line of Fig. 8, is given by Eq. (2).

$$C = 2.5 \cdot 10^{-2} \cdot f_{ev} \tag{2}$$

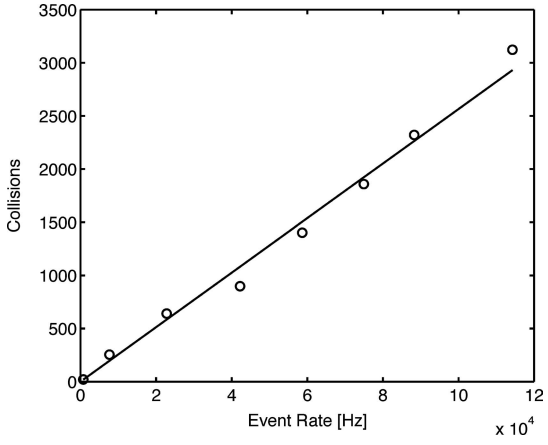

Fig. 8 Measured contention rate versus load for image sensor ALOHAim2

3. Results

The ALOHA image sensors employ an N-diffusion over P-substrate photodiode. The photodiode area is 63 μm^2. The photodiode response is given in Fig. 9, where photocurrent is measured as a function of typical indoor lighting conditions.

The photocurrent I_{ph} was computed from the firing rate (data in Fig. 11) using Eq. (3) [10]. Here C_{int} is the integration capacitance inside each pixel, V_{thp} is the event threshold (generally close to the threshold of a PMOS transistor in the process [41]), f_{event} is the output event rate from a specific pixel.

$$I_{ph} = C_{int} V_{thp} f_{event} \tag{3}$$

Figure 10 reports the dark signal I_{dc} of the ALOHA image sensor photodiode and event generator as a function of the reset voltage V_{ddr} (reverse bias).

The dark signal was measured by using Eq. (3) for a single pixel in the dark while varying the reset voltage. The solid line in Fig. 10 is given by Eq. (4).

$$I_{dc} = 42.55 - 12 \cdot V_{ddr}[fA] \tag{4}$$

The dark signal here reported is an average form the entire array. The dark signal is decreasing with increasing reverse bias, which is contrary to diode operation theory. This can be explained by inspecting the reset PMOS in Fig. 3. This PMOS switch will incur in an increase in leakage current when its drain to source voltage is increased (when V_{ddr} increases). This leakage current subtracts to the photodiode dark current effectively reducing the dark event rate of the pixels. Therefore the dark current is not decreasing with increasing bias, but instead is reduced by effect of the leakage

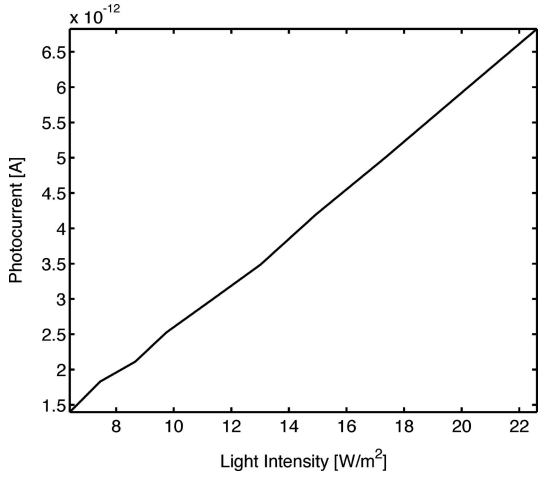

Fig. 9 Sensor photodiode response for the ALOHA image sensors in different indoor lighting conditions

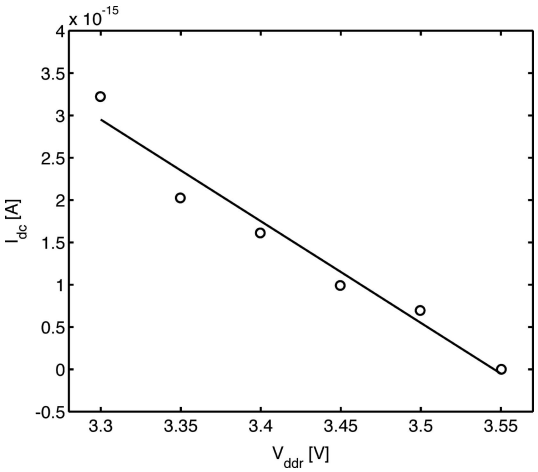

Fig. 10 Event generator dark signal for the ALOHA image sensors as a function of the reset voltage

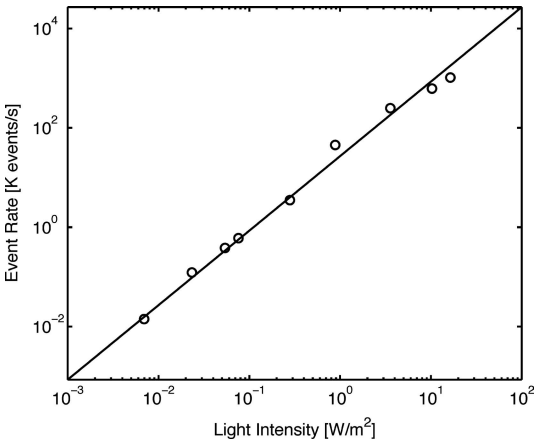

Fig. 11 Event rate of a patch of 3×4 pixels of ALOHAim1 image sensor as a function of illumination intensity

of the reset PMOS transistors. This is an interesting feature that can be exploited in event-based pixels to reduce the spurious dark response.

3.1. ALOHAim1 results

A die micrograph of ALOHAim1 is reproduced in Fig. 14. The sensor core size measures 1.2×1.2 mm, excluded the pad frame. With the pad frame (21 pads) the image sensor occupies an area of 1.5×1.5 mm. We measured the dynamic range of the image sensor by measuring the spike rate in the dark and with high illumination. In the dark the sensor produced a single event after 120 s. The equivalent dark rate for a single pixel is thus 8.13 μHz (since there are 32×32 pixels in the array). With very bright illumination, the image sensors minimum cycle time was 100 ns, for a rate of 10 MHz. Assuming a single pixel can fire at this rate if we focus light onto it, the measured dynamic range for an individual pixel is 240 dB. On the other hand, under uniform

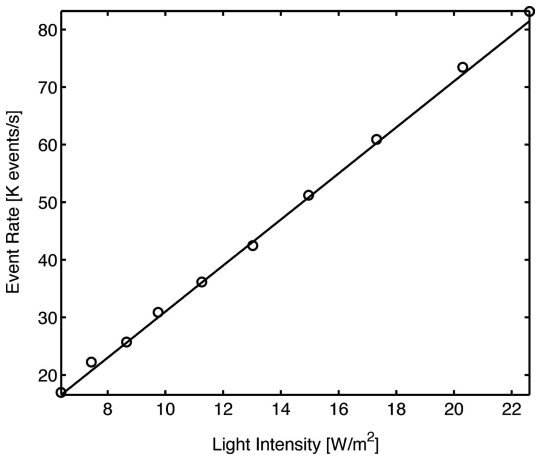

Fig. 12 Event rate of the ALOHAim1 array as a function of illumination intensity

illumination, the array has a dynamic range of 180 dB (8.33–10 MHz). This figure is instead of interest and it shows that event-based image sensor can provide about three times (in dB!) the performance of standard APS CMOS image sensor [6, 43]. This image sensor also improves on the dynamic range of several other research prototypes [4, 10, 20, 48–51].

Figure 11 reports the dynamic range of the event rate f_{ev} for a patch of 3×4 pixels, as a function of the illumination intensity I_{ill}. The solid line in Fig. 11 is given by Eq. (5).

$$f_{ev} = 27 \cdot I_{ill}^{1.5} \tag{5}$$

Illumination was varied using a high intensity lamp attenuated by neutral density filters. The light intensity was measured with a commercial photometer. Figure 12 shows the event of the entire pixel array F_{ev} as a function of typical indoor illumination I_{ill}. The solid line in Fig. 12 is given by Eq. (6).

$$F_{ev} = 4 \cdot I_{ill} - 9 \tag{6}$$

Table 1 summarizes the main characteristics of the array. The *sensitivity* is a cumulative performance metric of this image sensor [10]. Fixed pattern noise was measured in the dark as standard deviation to mean ratio of the array's

Fig. 13 Example images collected from ALOHAim1. President Jackson and text 'Fil'. Images were collected with the sensor operating at approximately 10 K events/s

Table 1 Summary of image sensor ALOHAim1 characteristics

Technology	0.6 μm 3 M CMOS
Array size	32×32
Pixel size	32.7×29.7 μm
Fill factor	6.5%
Sensor core size	1.2×1.2 mm
Bandwidth	8.13 μHz–10 MHz (Pixel)
	8.33 mHz–10 MHz (Array)
Throughput	110 Mbits/s (11 bits)
Dynamic range	241 dB (Pixel)
	181 dB (Array)
Sensitivity [Hz/W/m^2]	1.7×10^3 (Array)
	2.8×10^9 (Pixel)
FPN	4.36% (dark)
Max. FPS	4.88 K (effective)
Digital power	115 μW at 3.30 V
Analog power	680 μW at 3.30 V

histogram after collecting 100 K samples. The maximum reported frame rate supposes the use of interevent-imaging technique [10].

With the rail voltage setting of: $V_{ddd} = 3.3$ V, $V_{dda} = 3.3$ V, $V_{ddr} = 3.7$ V, the image quality and dynamic range was at its maximum. Power consumption of the image sensor in uniform room light (~0.1 mW/cm^2) is 680 μW for the analog supply and 115 μW for the digital supply, at a rate of 10 k events/s and cycle time of 350 ns. This data was collected while imaging connected to a receiving computer. A great majority of the power dissipation is due to the pseudo-CMOS logic used in this design. The digital power consumption can be improved by removing all pseudo-MOS logic devices (see ALOHAim2 in Section 3.2). At the maximum output event rate of 10 MHz the sensor array provided an output aggregated address bandwidth of 110 Mbits/s on the 5 X, 5 Y address lines and the request.

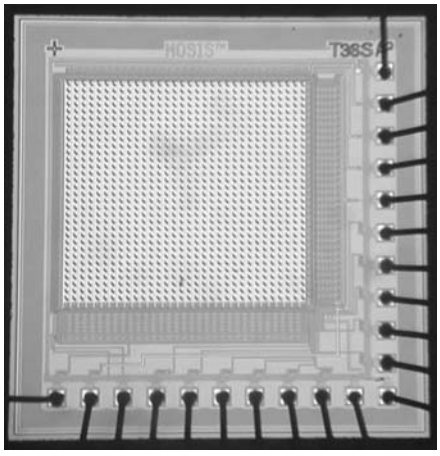

Fig. 14 Micrograph of the ALOHAim1 image sensor die. The die size is 1.5×1.5 mm and the core size is 1.2×1.2 mm. The MOSIS Fab-ID is T36RDN

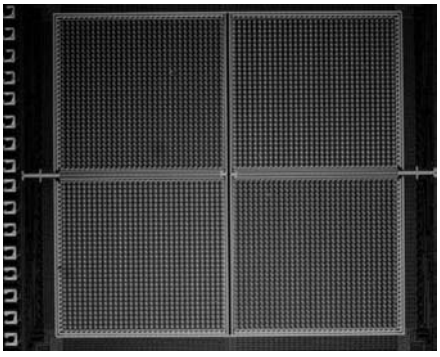

Fig. 15 Micrograph of the ALOHAim2 image sensor die. The die size is 3×3 mm and the core size is 2.4×2.4 mm. The MOSIS Fab-ID is T46TDN

Figure 13 shows example images recorded with the array and reconstructed using histogram normalization.

The image sensor is capable of updating its picture at a rate of 4.88 K frames/s.

3.2. ALOHAim2 results

A die micrograph of ALOHAim2 is reproduced in Fig. 15. Notice the four image quadrants. The sensor core size measures 2.4×2.4 mm, excluded the pad frame. With the pad frame (84 pads) the image sensor occupies an area of 3×3 mm. Each quadrant of the image sensor has the same dimensions and interface as ALOHAim1.

The equivalent dark rate for a single pixel is 8.13 μHz (one quadrant). With very bright illumination, the image sensors minimum cycle time was 200 ns, for a rate of 5 MHz at 3.3 V. Assuming a single pixel can fire at this rate if we focus light onto it, the measured dynamic range for an individual pixel is 235 dB. Similarly, under uniform illumination, the array has a dynamic range of 175 dB (8.33–5 MHz). Table 2 summarizes the main characteristics of the array. Fixed pattern noise was measured in the dark as standard deviation to mean ratio of the array's histogram after collecting 100 K samples. The maximum reported frame rate supposes the use of interevent-imaging technique [10].

Although the sensor was designed for a 3.3 V power supply (digital analog and pixel reset), the image quality was improved significantly by running at an operating voltage of 2.35 V for V_{dda} and V_{ddd} and 2.65 V for V_{ddr}. Two samples collected, respectively of the 'analog devices' sign and president Jackson of a 20 dollars bill are reported in Fig. 16. The image sensors produced approximately 10,000 events in a period of 1375 ms for both samples in Fig. 16. The images were reconstructed using the histogram normalization. Figure 17 shows an image of the Yale engineering logo collected using all four quadrants on ALOHAim2 sensor. The image size composite is 64×64 pixels.

Table 2 Summary of ALOHAim2 image sensor characteristics

Technology	0.6 μm 3 M CMOS
Array size	64 × 64 (4 quadrants of 32 × 32)
Pixel size	32.7 × 29.7 μm
Fill factor	6.5%
Sensor core size	2.4 × 2.4 mm (4 quadrants)
Bandwidth	8.13 μHz–5 MHz (Pixel)
	8.33 mHz–5 MHz (Array)
Throughput	55 Mbits/s (one quadrant 11 bits)
	220 Mbits/s (4 quadrant 44 bits)
Dynamic range	235 dB (Pixel)
	175 dB (Array)
Sensitivity [Hz/W/m^2]	5.6 × 10^5 (Array)
	9.1 × 10^{11} (Pixel)
FPN	4.36% (dark)
Max. FPS	2.44 K (effective)
Digital power	5.75 μW at 2.35 V
Analog power	3.9 nW at 2.35 V

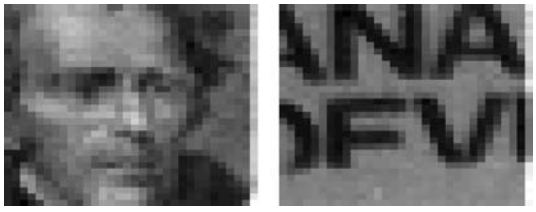

Fig. 16 Example images collected with image sensor ALOHAim2. President Jackson and 'Analog Devices' text. Images were collected with the sensor operating at 7.6 K events/s

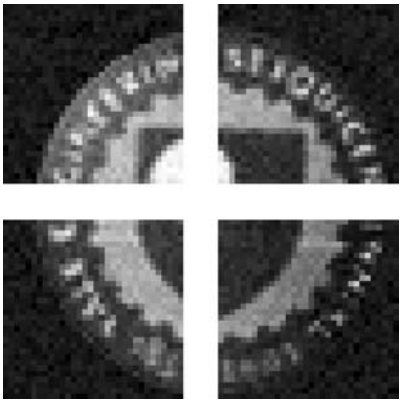

Fig. 17 Image taken with all four quadrants of ALOHAim2

The current consumption of each quadrant for this output event rate was 2.5 μA for the digital supply and 2.8 nA and 1.1 nA respectively for the analog and pixel reset supplies. This corresponds to a power consumption of 5.75 μW for each quadrant of ALOHAim2. Figure 18 reports the power consumption (P_c) of one quadrant of the image sensor as a function of the event rate, for typical indoor lighting conditions. Equation (7) represents the solid line in Fig. 18.

$$P_c = 1.1 \cdot f_{ev}[nW] \tag{7}$$

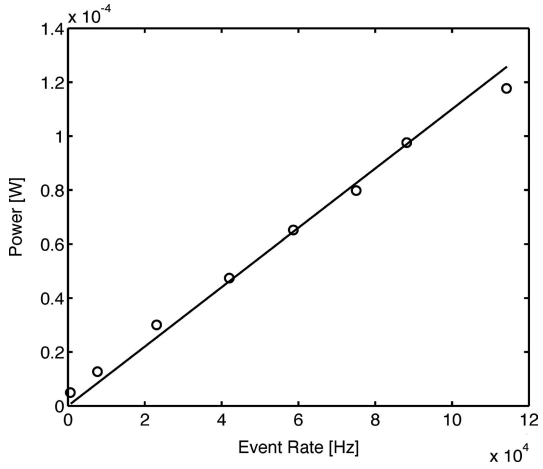

Fig. 18 Power consumption of one quadrant of ALOHAim2 versus its event rate under typical indoor lighting conditions

Since a frame can be though as two events for each of the 32 by 32 pixels, the frame rate was 3.51 fps. The maximum event rate for ALOHAim2 is 2 Ms/s at 2.35 V and 5 Ms/s at 3.3 V. At 2 Ms/s and 2.35 V operation, the current consumption was 0.24 mA for the digital supply and 1.5 umA for the analog power supply. This corresponds to a frame rate of respectively 976 fps and 2441 fps. The image sensor is capable of updating its picture at a rate of 2.44 K frames/s.

At the maximum output event rate of 5 MHz the sensor array provided an output aggregated address bandwidth of 220 Mbits/s on the four quadrant's 5 X, 5 Y address lines and the request. Each quadrant provided an address bandwidth of 55 Mbits/s.

4. Discussion and sensor networks applications

The field of sensor network finds its most appealing and natural applications in serving as a monitoring device for large-area deployment, where distributed sensing has to be autonomous. In this regard, monitoring of large natural environments is a typical application [24–27]. Life sciences [28], forestry and environmental studies can be accomplished by monitoring the presence or lack of targets, like animals, natural events, toxical elements [29].

Monitoring of large environments include man-made environments like bridges, streets, highways, city blocks and urban areas. Sensor network facilitate monitoring of highway traffic, transportation statistical measurements, human presence, statistical collection of data for intersection lights, street crosswalks, traffic [32]. Buildings and other civil structures as bridges are often monitored for stability, aging statistics, usage statistics, operational status.

Monitoring human presence in a large area has interest for security and counter-terroristic measures, and has been

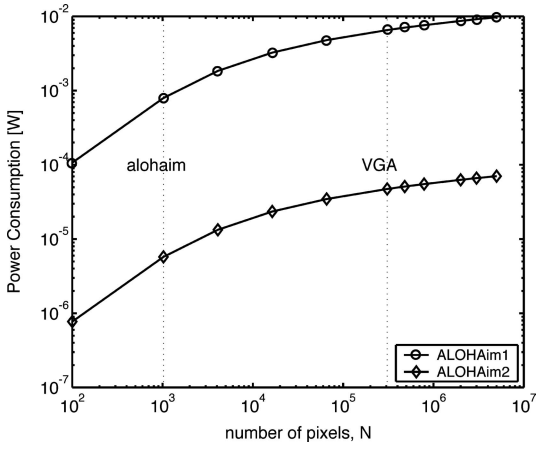

Fig. 19 Power consumption scaling properties for the ALOHA image sensors

proven more and more of interest in the recent years [30, 31]. In war-zones, it is invaluable to be able to monitor large area for presence of hostile forces.

While some of the above mentioned applications can be solved using a network employing a variety of different sensors, all of the mentioned application can be solved using an image sensor network. Important image sensor specifications required for sensor network applications are:

- Low-power operation (<1 mW)
- High dynamic range (>100 dB)
- Digital interface
- Few or no external components
- Data compression at sensor level
- Low cost
- Fast readout

The ALOHA image sensors possess all of the above requirements and are thus perfect for the above-mentioned applications. In particular, with a current consumption of 2.5 μA ALOHAim2 can run on two 1000 mAh AA batteries for 4.5 years! Figure 19 reports the scaling properties of the power consumption of image sensor ALOHAim2 in comparison to ALOHAim1. The scaling properties are derived from Eq. (8). The power consumption P_N scales with the number of pixels N as in Eq. (8). N_0 and P_{N_0} are respectively the number of pixel (32×32) and the power consumption of the ALOHAim1 image sensor. The power scales as the $\log_2$ of N because the power consumption is directly proportional to the number of output digital lines (see Sections 3 and 3.2).

$$P_N = P_{N_0} log_2\left(1 + \frac{N}{N_0}\right) \tag{8}$$

Notice that the ALOHAim2 sensor can operate with as little as 50 μW and VGA size, making it the lowest power image sensor yet reported in the literature. The large dynamic range in the excess of 200 dB allows the ALOHA image sensors to perform almost as well as the human eye in different illumination settings [52, 53]. Note that the dynamic range of the ALOHA image sensors array decreases with the number of pixels, as can be seen in Fig. 20 and Eq. (9). Even at VGA sizes the ALOHA image sensors have enough dynamic range to be able to operate over a large scale of illumination settings. ALOHAim2 has a lower dynamic range than ALOHAim1 because of its lower maximum output rate (see Section 3.2). The dynamic range DR_N scales with the number of pixels N as in Eq. (9). $\mathrm{PF}_{\max}$ and $\mathrm{PF}_{\min}$ are respectively the maximum and minimum event rates of the ALOHAim1 image sensor. The dynamic range scales inversely proportional to N because pixels share the maximum chip output bandwidth.

$$DR_N = 20 log_{10}\left(\frac{PF_{\max}}{PF_{\min}}\frac{N_0}{N}\right) \tag{9}$$

The digital interface with no external components (ALOHAim2 requires only a single power supply) simplifies the interface with sensor network nodes. The compression of data or the selective readout offered by the address-event representation of the ALOHA imagers make efficient use of the output bandwidth [41]. Note that image noise (measured as 5% rms [11]) is due to the lack of fixed pattern noise (FPN) cancelation circuits in temporal domain. FPN cancelation circuits like correlated double sampling (CDS) circuits are used in most CMOS APS imagers. This high levels of noise are not an issue for many distributed sensor network application, when the output of many sensor can be combined constructively. The fast readout rates of the ALOHA image sensors can be used to monitor fast moving objects or events when required. In order to decrease the readout rate of the sensor the readout acknowledge can be used to stall the sensor. This way the sensor will not require bulky mechanical shutters and can be packaged in a small, unnoticeable volume.

On a final note, even if the sensor node report ultra-low power operation, the conjunction of this sensor with a sensor network node will not be able to operate at this power levels if data is continuously read and transmitted. In fact a transmitting sensor network node consumes 70 mW of power (Berkeley MICAZ mote). The same node will consume 30 mW of power when the processor is active. Our sensor is the first step in the creation of a series of vision wake-up triggers for sensor network nodes. Our sensors currently only detects pixel intensity, but we are working on a motion detector based on intensity differences in the image. The idea is to keep the sensor network node in a low-power sleep mode (consuming a few μW) until the sensor detects action in the scene. In this case the low-power feature of the sensor is necessary to keep the sensor network node operating for extended periods of time, since only the sensor is

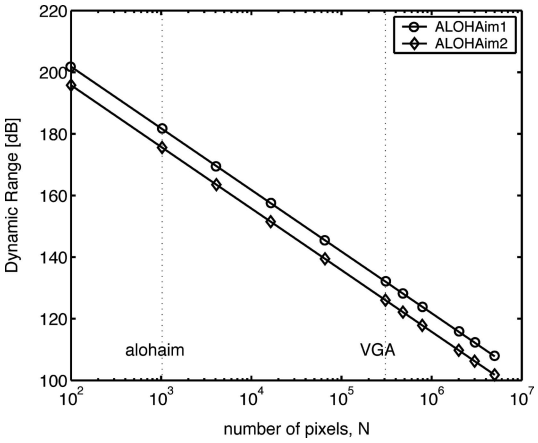

Fig. 20 Power consumption scaling properties for the ALOHA image sensors

always active and the node is only turned-on for short periods of time.

5. Summary

We fabricated and tested a 32×32 pixels digital address-event imager with analog contention detection and a 64×64, four quadrants sensor with digital collision detection. The ALOHAim1 image sensor core size measures 1.2×1.2 mm and provides a dynamic range of 240 dB, a low power consumption of 795 μW and is capable of updating its image at a rate of 4.88 K frames/s. The ALOHAim2 image sensor core size measures 2.4×2.4 mm and provides a dynamic range of 235 dB, a low power consumption of 5.75 μW and is capable of updating its image at a rate of 2.44 K frames/s. Both image sensor are one of the largest dynamic range [4, 10, 11, 40], lowest power [5] and fastest [39] in the literature. The performance of these sensors make them an ideal low-resolution image sensor for sensor networks applications.

Acknowledgments Fabrication was provided by MOSIS. This work was supported in part by the National Science Foundation grants *Integrated Sensing: Cell clinics on a chip, ECS-0225489* and *A Comparative Study of Information Processing in Biological and Bio-inspired Systems: Performance Criteria, Resources Tradeoffs and Fundamental Limits, EIA-0130812*.

References

1. Y. Liu, W. Gao, H. Yao, S. Liu, and L. Wang, "Fast moving region detection scheme in ad hoc sensor network." In *Proceedings Lecture Notes In Computer Science*, vol. 3212, pp. 520–527, 2004.
2. E.M.C.F. Chiasserini, "Energy-efficient coding and error control for wireless video-surveillance networks." *Telecommunication Systems*, vol. 26, pp. 369–387, 2004.
3. M. Tehrani, P. Bangchang, T. Fujii, and M. Tanimoto, "The optimization of distributed processing for arbitrary view generation in camera sensor networks." *IEICE Transactions On Fundamentals Of Electronics Communications And Computer Sciences*, vol. 8, pp. 1863–1870, 2004.
4. W. Yang, "A wide-dynamic range, low-power photosensor array," In *IEEE International Solid-State Circuits Conference, ISSCC*, San Francisco, CA, 1994, pp. 230–231.
5. K. Cho, "A 1.2 V micropower CMOS active pixel image sensor for portable applications." In *IEEE International Solid-State Circuits Conference, ISSCC*, San Francisco, CA, 2000, pp. 114–115.
6. K. Cho, A. Krymski, and E. Fossum, "A 1.5-V 550-μW 176×144 autonomous CMOS active pixel image sensor." *IEEE Transactions on Electron Devices*, vol. 50, no. 1, pp. 96–105, 2003.
7. Various authors, In *Proceedings of IEEE Special Issue on Sensor Networks*. IEEE, Aug. 2003.
8. P. Julian, A. Andreou, L. Riddle, S. Shamma, and G. Cauwenberghs, "A comparative study of sound localization algorithms for energy aware sensor network nodes." *IEEE Transactions On Circuits And Systems I: Regular Papers*, vol. 51, pp. 640–648, April 2004.
9. K.A. Boahen, "Point-to-point connectivity between neuromorphic chips using address events." *IEEE Trans. Circuits and Systems-II: Analog and Digital Signal Processing*, vol. 47, no. 5, pp. 416–434, 2000.
10. E. Culurciello, R. Etienne-Cummings, and K.A. Boahen, "A biomorphic digital image sensor." *IEEE Journal of Solid-State Circuits*, vol. 38, no. 2, pp. 281–294, 2003.
11. E. Culurciello and R. Etienne-Cummings, "Second generation of high dynamic range, arbitrated digital imager." In *IEEE International Symposium on Circuits and Systems, ISCAS*, vol. 4, Vancouver, Canada, 2004, pp. IV–828–31.
12. N. Abramson, "THE ALOHA SYSTEM—a nother alternative for computer communications." In *Proc. 1970 Fall Joint Computer Conference*, 1970, pp. 281–285.
13. B. Leibowitz, B. Boser, and K. Pister, "CMOS "smart pixel" for free-space optical communication." In *Proceedings SPIE*, vol. 4306, *SPIE*, 2001, pp. 308–318.
14. B. Warneke, M. Last, B. Liebowitz, and K. Pister, "Smart dust: communicating with a cubic-millimeter computer." *Computer*, vol. 34, pp. 44–51, 2001.
15. SMal Camera Technologies, "IM-001 model series," URL http://www.smalcamera.com/.
16. Micron semiconductors. "Model MT9V012," URL http://micron.com/products/imaging/.
17. Agilent Camera Modules and Image Sensors, "Model ADCM-1650-3011" URL http://www.home.agilent.com/.
18. C. Fermuller, Y. Aloimonos, P. Baker, R. Pless, J. Neumann, and B. Stuart, "Multi-camera networks: eyes from eyes." In *Proceedings of IEEE Workshop on Omnidirectional Vision, 2000*, 2000, vol. 12, pp. 11–18.
19. P. Doubek, I. Geys, T. Svoboda, and L.V. Gool, *Cinematographic Rules Applied to a Camera Network*. Omnivis, 2004.
20. L. McIlrath, "A low-power low-noise ultrawide-dynamic-range CMOS imager with pixel-parallel A/D conversion." *IEEE Journal of Solid-State Circuits*, vol. 36, no. 5, pp. 846–853, 2001.
21. M. Rahimi, D. Estrin, R. Baer, H. Uyeno, and J. Warrior, "Cyclops: image sensing and interpretation in wireless networks." In *Second ACM Conference on Embedded Networked Sensor Systems, SenSys*, Baltimore, MD, 2004.
22. T. Ko and N. Berry, "Distributed feature extraction for event identification." In *Ambient Intelligence: Second European Symposium, EUSAIP roceedings*, vol. 3295. Eindhoven, The Netherlands,

2004, pp. 136–147.
23. PASTA, *PASTA Microsensor 1.0 Developers Manual*, USC ISI, 2005, http://pasta.east.isi.edu/
24. D. Hymer, "Soil water evaluation using a hydrologic model and calibrated sensor network." *Soil Science Society of America Journal*, vol. 64, pp. 319–327, 2000.
25. M. Goodchild, "Geographic information science and systems for environmental management." *Annual Review of Energy and the Environment*, vol. 28, p. 493, 2003.
26. K. Yun et al., "A miniaturized low-power wireless remote environmental monitoring system based on electrochemical analysis." *Sensors and Actuators B: Chemical*, vol. 102, pp. 27–35, 2004.
27. R. Szewczyk, E. Osterweil, J. Polastre, M. Hamilton, A. Mainwaring, and D. Destrin, "Habitat monitoring with sensor networks." *Communications of the ACM*, vol. 47, pp. 34–41, 2004.
28. J. Kumagai, "The secret life of birds." *IEEE Spectrum*, vol. 41, pp. 42–50, 2004.
29. R.J. Nemzek and J. Dreicer, "Distributed sensor networks for detection of mobile radioactive sources." *IEEE Transactions on Nuclear Science*, vol. 51, pp. 1693–1701, 2004.
30. R. Brooks, D. Friedlander, J. Koch, and S. Phoha, "Tracking multiple targets with self-organizing distributed ground sensors." *Journal of Parallel and Distributed Computing*, vol. 64, pp. 874–885, 2004.
31. K. Morioka, J. Lee, and H. Hashimoto, "Human-following mobile robot in a distributed intelligent sensor network." *IEEE Transactions on Industrial Electronics*, vol. 51, pp. 229–238, 2004.
32. M. Duarte and H. Yu, "Vehicle classification in distributed sensor networks." *Journal of Parallel and Distributed Computing*, vol. 64, pp. 826–839, 2004.
33. E. Culurciello and A.G. Andreou, "ALOHA CMOS imager." In *IEEE International Symposium on Circuits and Systems, ISCAS*, Vancouver, Canada, 2004, pp. IV–956–9.
34. C. Mead and M. Mahowald, *A Silicon Model of Early Visual Processing*. Pergamon Press, 1988.
35. M. Sivilotti, "Wiring considerations in analog VLSI systems with applications to field programmable networks." Ph.D. dissertation, California Institute of Technology, 1991.
36. A. Andreou and K. Boahen, "A 590,000 transistor, 48,000 pixel contrast sensitive, edge enhancing CMOS imager-silicon retina." In *Preceedings of the 16th Conference on Advaced Research in VLSI*, Chapel Hill, NC, 1995, pp. 225–240.
37. Z. Kalayjian and A. Andreou, "Asynchronous communication of 2d motion information using winnertake-all arbitration," *Journal of Analog Integrated Circuits and Signal Processing*, vol. 103–109, p. 13, 1997.
38. K. Boahen, *Communicating Neuronal Ensembles Between Neuromorphic Chips, Neuromorphic Systems Engineering*. Kluwer Academic Publishers, ch. 11, pp. 229–261, 1998.
39. N. Stevanovic, "A CMOS image sensor for high-speed imaging." In *IEEE International Solid-State Circuits Conference, ISSCC*, San Francisco, CA, 2000, pp. 104–105.
40. O. Yadid-Pecht and A. Belenky, "In-pixel autoexposure CMOS APS." *IEEE Journal of Solid-State Circuits*, vol. 38, pp. 1425–1428, 2003.
41. E. Culurciello and A. Andreou, "A comparative study of access topologies for chip-level address-event communication channels." *IEEE Transactions On Neural Networks*, vol. 14, pp. 1266–1277, 2003 (special Issue On Hardware Implementations).
42. K. Boahen, "Retinomorphic vision systems." *IEEE MicroNeuro*, pp. 2–14, 1996.
43. E. Fossum, "CMOS image sensors: Electronic camera-on-a-chip." *IEEE Transactions on Electron Devices*, vol. 44, no. 10, pp. 1689–1698, 1997.
44. S. Kleinfelder, S. Lim, X. Liu, and A.E. Gamal, "A 10000 frames/s CMOS digital pixel sensor." *IEEE Journal of Solid-State Circuits*, vol. 36, no. 12, pp. 2049–2059, 2001.
45. A. Mortara and E. Vittoz, "A communication architecture tailored for analog VLSI artificial neural networks: Intrinsic performance and limitations." *IEEE Transactions on Neural Networks*, vol. 5, no. 3, pp. 459–466, 1994.
46. A. Mortara, E. Vittoz, and P. Venier, "A communication scheme for analog VLSI perceptive systems." *IEEE Journal of Solid-State Circuits*, vol. 30, no. 6, pp. 660–669, 1995.
47. M.M.A. Abusland and T. Lande, "A VLSI communication architecture for stochastically pulse-encoded analog signals." *IEEE International Symposium of Circuits and Systems, ISCAS*, Atlanta, Georgia, vol. 3, pp. 401–404, 1996.
48. O. Yadid-Pecht and E. Fossum, "Wide intrascene dynamic range CMOS APS using dual sampling." *IEEE Transactions on Electron Devices*, vol. 44, no. 10, pp. 1721–1723, 1997.
49. D. Yang, A.E. Gamal, B. Fowler, and H. Tian, "A 640×512 CMOS image sensor with ultrawide dynamic range floating-point pixel-level ADC." *IEEE Journal of Solid-State Circuits*, vol. 34, pp. 1821–1833, 1999.
50. O. Schrey, R. Hauschild, B. Hosticka, U. Lurgel, and M. Schwarz, "A locally adaptive CMOS image sensor with 90 dB dynamic range." In *IEEE International Solid-State Circuits Conference, ISSCC*, 1999, pp. 310–311.
51. M. Schanz, C. Nitta, A. Bubmann, B. Hosticka, and R. Wertheimer, "A high-dynamic-range CMOS image sensor for automotive applications." *IEEE Journal of Solid-State Circuits*, vol. 35, pp. 932–938, 2000.
52. D. Hubel, *Eye, Brain, and Vision*. Scientific American Library (HPHLP), 1988.
53. B. Wandell, *Foundations of Vision*. Sinauer Associates Inc. Publishers, 1995.

Eugenio Culurciello (S'97–M'99) received the Ph.D. degree in Electrical and Computer Engineering in 2004 from Johns Hopkins University, Baltimore, MD. In July 2004 he joined the department of Electrical Engineering at Yale University, where he is currently an assistant professor. He founded and instrumented the E-Lab laboratory in 2004. His research interest is in analog and mixed-mode integrated circuits for biomedical applications, sensors and networks, biological sensors, Silicon on Insulator design and bio-inspired systems.

Andreas G. Andreou received his Ph.D. in electrical engineering and computer science in 1986 from Johns Hopkins University. Between 1986 and 1989 he held post-doctoral fellow and associate research scientist positions in the Electrical and Computer engineering department while also a member of the professional staff at the Johns Hopkins Applied Physics Laboratory. Andreou became an assistant professor of Electrical and Computer engineering in 1989, associate professor in 1993 and professor in 1996. He is also a professor of Computer Science and of the Whitaker Biomedical Engineering Institute and director of the Institute's Fabrication and Lithography Facility in Clark Hall. He is the co-founder of the Johns Hopkins University Center for Language and Speech Processing. Between 2001 and 2003 he was the founding director of the ABET accredited undergraduate Computer Engineering program. In 1996 and 1997 he was a visiting professor of the computation and neural systems program at the California Institute of Technology. In 1989 and 1991 he was awarded the R.W. Hart Prize for his work on mixed analog/digital integrated circuits for space applications. He is the recipient of the 1995 and 1997 Myril B. Reed Best Paper Award and the 2000 IEEE Circuits and Systems Society, Darlington Best Paper Award. During the summer of 2001 he was a visiting professor in the department of systems engineering and machine intelligence at Tohoku University. In 2006, Prof. Andreou was elected as an IEEE Fellow and a distinguished lecturer of the IEEE EDS society.

Andreou's research interests include sensors, micropower electronics, heterogeneous microsystems, and information processing in biological systems. He is a co-editor of the IEEE Press book: Low-Voltage/Low-Power Integrated Circuits and Systems, 1998 (translated in Japanese) and the Kluwer Academic Publishers book: Adaptive Resonance Theory Microchips, 1998. He is an associate editor of IEEE Transactions on Circuits and Systems I.